Development and characterization of outgassing rates for use in an expanded LIGO vacuum

A thesis submitted in partial fulfillment of the requirement
for the degree of Bachelor of Science in
Physics from the College of William and Mary in Virginia,

by

Samantha L. Cohodas

Advisor: Dr. William E. Cooke

Dr. Todd D Averett

Williamsburg, Virginia
May 2021

Contents

Acknowledgments

I would like to thank many people for assisting and preparing me as I complete this thesis. Primarily, Dr. William Cooke for advising and guiding me through our collective research. Professor Dennis Manos for his contributions and insight into to the research as well as being an additional resource through throughout. I would also like to thank my major advisor Professor Novikova and the rest of my physics professors at William & Mary for preparing me to graduate and imparting their physics knowledge upon me and my classmates.

List of Figures

List of Tables

Abstract

The purpose of this experiment is to determine the outgassing rates of various gasses from an AISI-1020 pipe in order to develop methodology to minimize those rates within a vacuum. The gasses being studied include hydrogen (H_2), methane (CH_4), water vapor (H_2O), carbon monoxide (CO), and carbon dioxide (CO_2). CO and CO_2 are of particular interest because they have higher atomic mass and concentrations within the pipe thus cause greater interference with high precision lasers like those at LIGO. The methodology is to measure background outgassing from the main chamber and pulsing gas from the AISI-1020 pipe. This is done at 21°C, 40°C, 50°C, 60°C, 70°C, and 80°C over the course of experimentation. The data is collected using a spinning rotor gauge (SRG), a residual gas analyzer (RGA), and a Baratron. By analyzing the background and pipe outgassing rates, one can determine the rate of rise (ROR) in pressure and the relationship to temperature. After being properly calibrated for the experimental device being used, this data is used to interpret a binding energy for the different gasses studied. Ultimately, the research will be useful in the next generation of LIGO experiments.

Chapter 1

Introduction

A vacuum is the absence of air and other gasses from a space. To create a vacuum, one must pump out all the gas molecules from inside of the vacuum space. However, soon after creating a vacuum, molecules from the sides of the vacuum container will come into the space through a process called outgassing. Outgassing can be measured through the pressure created by the gas molecules. How quickly outgassing occurs depends on multiple factors such as temperature, the material of the container that the vacuum is contained in and how the material is prepared, and the types of gasses that are outgassing off the walls.

Laser Interferometer Gravitational-wave Observatory (LIGO) currently consist of two interferometer detectors. Each interferometer is made two 4-kilometer vacuum arms that measure gravitational waves. A gravitational wave is detected by a disruption in the expected interference pattern created by a laser bouncing between mirrors in the vacuum arms. LIGO does have seismic isolation systems to eliminate some of the extraneous variables, however, gas particles outgassing off the vacuum walls can scatter the laser beam as well as collide with and move the mirrors of the interferometer which is not easily corrected [4].

The aim of this experiment is to measure the outgassing rates and determine which molecules contribute significantly to the total pressure. The system we are using is

testing AISI-1020 pipe which is a cheaper alternative by about a factor of 3 compared to using stainless steel [2][8]. Also, LIGO plans to build a detector with arms that are about 10 times as long called the Cosmic Explorer [1]. This much larger detector will require larger vacuums thus having more opportunities for outgassing [1]. By determining the outgassing rates and composition, we develop knowledge that can be used in the effort to minimize the outgassing thus minimizing interference of particles at LIGO.

Chapter 2

Experimental Methodology

2.1 Experimental Set-up and Procedure

This experiment works by measuring the pressure of the gas molecules as they outgas. Figure 2.2 shows a schematic of the experiment. Several instruments are used in this study including: residual gas analyzer (RGA), a spinning rotor gauge (SRG), and baratron. The RGA works by ionizing the gas molecules and then measuring the resulting charge to mass ratio and pressure based on calibration using the Baratron [9].Thus, the RGA provides information about the partial pressures produced by each gas as well as the overall gas composition. However, the RGA is sensitive to the gas used to calibrate which for our experiment is N_2. This means that the stated partial pressures are not representative of the true partial pressure and are off by a factor based on the cross-sectional area of the molecule compared to that of N_2 [3]. These values can be found in Table 2.1.

The spinning rotor gauge (SRG) measures pressure directly in the vacuum pipe using a small spinning ball that when particles collide with it, slows down in speed which is translated to a pressure in Torr [5]. The spinning rotor gauge measures the overall pressure in the pipe but is also calibrated to nitrogen gas, and is sensitive to the viscosity and temperature of the outgas as well [5]. To determine the true pressure

Molecule	Cross-Section in Å^2	Ratio to N_2
H_2	1.021	2.456
H_2O	2.275	1.102
CO	2.516	0.997
CO_2	3.521	0.712

Table 2.1: Cross-Sections and Ratios at 70eV
This table displays the cross-sections for H_2, H_2O, CO, and CO_2 in Å^2 using an incident energy of 70eV. This is using the Electron-Impact Ionization Cross Section for Ionization and Excitation Database [3]. It also displays the ratio of the cross-section of N_2 (2.508 Å^2) to the cross-section of each molecule because RGA is calibrated to nitrogen gas.

in the pipe, the relative molecular mass is needed and can be calculated based on the relative pressures of each gas present. The equation used is found in Fig. 2.1 [6]. This relative mass can than be compared to the mass of nitrogen gas and used to calibrate the SRG to a true pressure.

$$M_{res} = (a_1 \cdot \sigma_1 \cdot \sqrt{M(1)} + a_2 \cdot \sigma_2 \cdot \sqrt{M(2)} + ... a_n \cdot \sigma_n \sqrt{M(n)})^2$$

Figure 2.1: This is the equation for calculating the relative mass of a gas mixture [6]. For n = positive integers: *a(n)* is the fraction of the mixture that is the particular gas, *M(n)* is the mass of that particular gas, and $\sigma(n)$ is the accommodation factor of that particular which is assumed to be = 1 for all of our gas molecules.

There are two main components to this experiment: determining overall outgassing rate and determining gas composition. In order to collect overall outgassing rate, the AISI-1020 pipe pressure is pumped down to a vacuum, then the pressure is allowed to build as molecules outgas. This change in pressure is measured using the SRG over time, an example of which is shown in Fig. 2.3. Over long periods of time where the system is undisturbed, the SRG pressure increases linearly with respect to time providing steady information as to the overall outgassing rate in the pipe. This behavior changes and is further discussed in later sections.

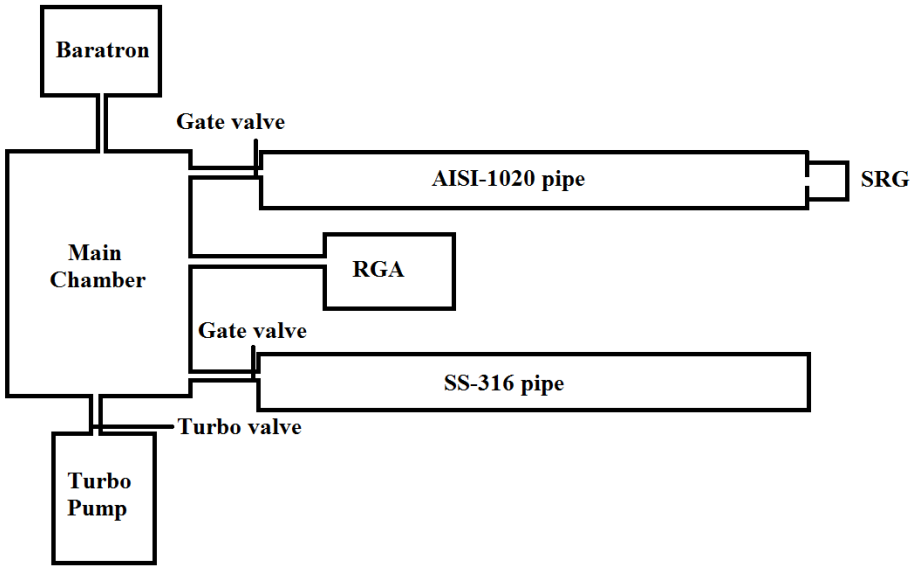

Figure 2.2: This figure is a schematic diagram of the outgassing experiment. This shows the location of gate valves as well as how the system is connected. The components are not to scale.

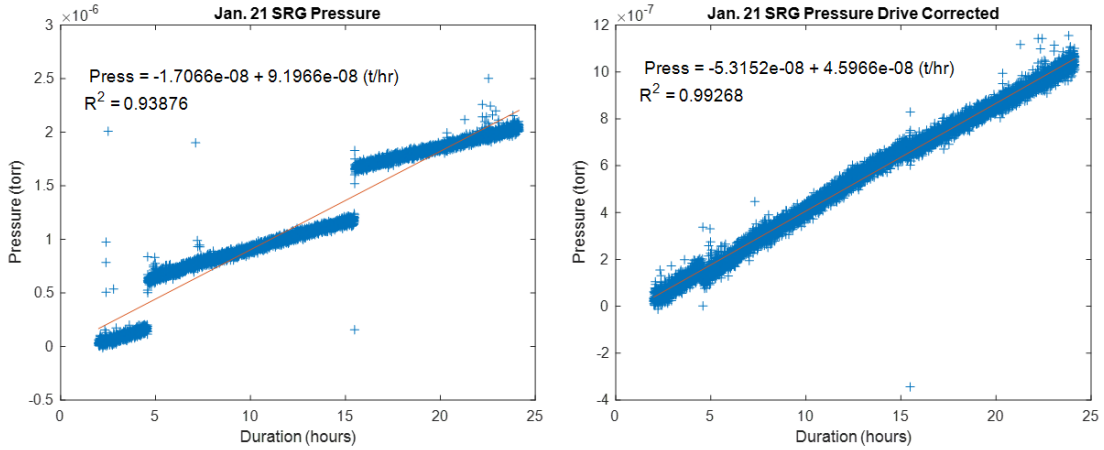

Figure 2.3: This is a example of SRG pressure collected over time starting on January 21^{st}, 2021. The data has periodic breaks in the otherwise linear relationship. These breaks are due to the SRG drive turning on to increase the spin velocity of the internal ball. This causes a jump in pressure of 5 x 10^{-7} Torr. The plot on the left is displaying the raw SRG data while the plot on the right is displaying the same data but corrected for the drive turning on. Without the breaks due to the drive, the SRG rises at a steady linear rate over time as shown on the right.

In order to determine the gas composition within the pipe, the pipe gas must be let into the main chamber in order to be measured by the RGA. First, the main chamber is pumped down using the turbo pump. Then, the turbo valve is closed, and the main chamber outgasses and is measured using the RGA. These two steps are repeated multiple times to establish background outgassing rates. After several background scans, the gate valve is open momentarily to pulse in the pipe gas to be measured by the RGA. Then the system is pumped down again by opening the turbo valve. The cycle of background scans followed by letting in the pipe gas continues once or twice more. The RGA can read data in one of two ways. The first way is a full scan of the atomic mass spectra from 1-50 which is referred to as a "standard RGA" run and is plotted on an AMU vs. pressure graph. Figure 2.4 shows an example standard RGA run. The second way is a specialized run where the RGA preforms a slower scan rate around the major AMU peaks and a faster scan rate over the rest of the AMU values. This is referred to as a "P vs. T" because it measures pressure over time of particular AMU values. The P vs. T collects more data points in a shorter amount of time for specific AMU values than the standard RGA run and plots the pressure of each AMU value over time. Figure 2.5 shows an example P vs. T graph for AMU 2. This is relevant because the pressure of each gas changes rapidly once the RGA filament is on and the pipe gases are let in. Because the goal is to determine what was in the AISI-pipe originally, the P vs. T graph allows for more accurate extrapolation to time 0. For both methods, the goal is determine the composition of the gasses and how much of each gas is from the main chamber outgassing. Lastly, there is a modified P vs. T method where same procedure is followed but the pipe is heated to various temperatures. For these studies, the temperature was raised sequentially on the thermocouples, which are attached to the AISI-1020 pipe, to 40°C, 50°C, 60°C, 70°C, and 80°C. Then, both the pipe gasses from the pulse and the background gasses

are measured using the same process as described above. The only exception is the 70°C and 80°C studies where the background scans occurred after the pulsed scans due to the rapid increase in SRG pressure.

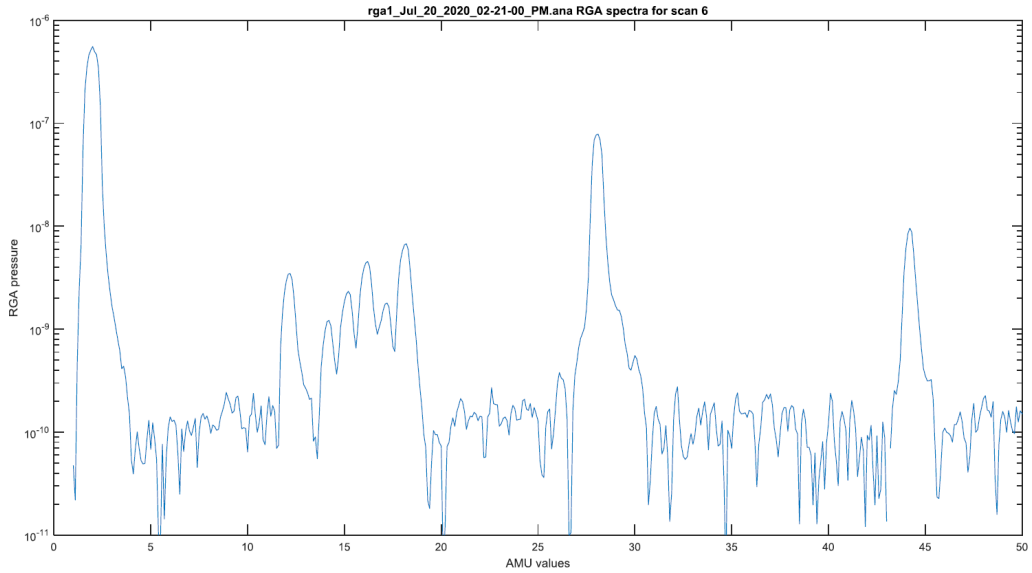

Figure 2.4: This is a sample of a standard RGA run for background or main chamber outgassing only. This graph shows AMU values vs. pressure in Torr. As shown on the graph, the major peaks occur at AMU 2, 12, 14, 15, 16, 18, 28, and 44. These are the peaks of focus because they make up the largest percent of the outgassing. This graphs shows the magnitude of the peaks as measured by the RGA but not as corrected using the cross-section of the gas molecules.

2.2 Challenges in Data Collection

Due to the nature of the experiment there are some difficulties when collecting data to determine the outgassing rates of different gasses. These challenges have influenced the current procedure for data collection. Primarily, the system is time dependent, and to determine how much of each gas was in the pipe initially when it was pulsed into the main chamber requires backwards extrapolation from the pipe burp and forwards extrapolation from the background outgassing to time 0. This is

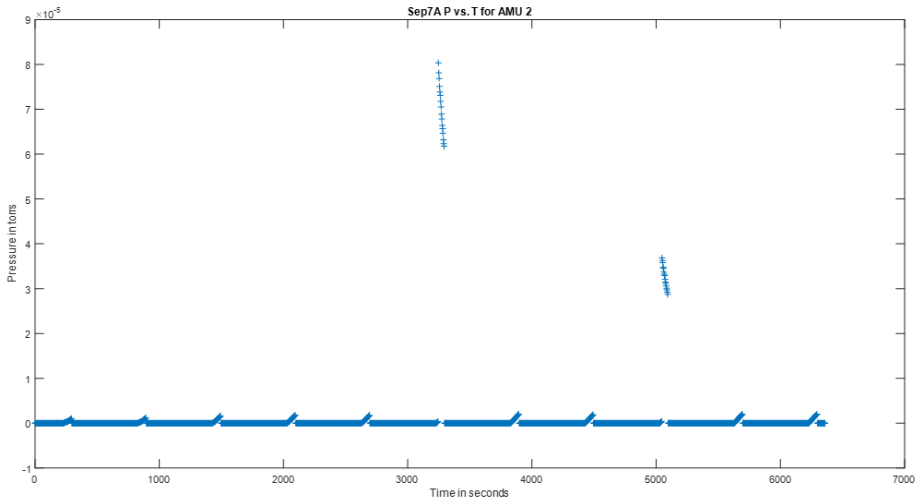

Figure 2.5: This is a sample P vs. T Graph for AMU 2 from September 7^{th} 2020. The RGA calibrated pressure is plotted over time. The two places where the pressure is high and the slope is negative are after the AISI-1020 pipe gas is pulsed in. The places where the pressure is low but increases are background scans where just the main chamber is outgassing. This demonstrated that the background outgassing is minimal compared to the AISI-1020 pipe.

why the P vs. T runs are particularly useful because the method collects more data points for the same amount of time and thus better shows the change in concentration. The changes in concentrations are likely due to the RGA heated filament used to ionize the gases. This filament likely reacts with the gas molecules causing chemical reactions which changes the composition of the outgas. It is difficult to eliminate the chemical reactions occurring due to the filament hence why extrapolating to time 0 provides the most accurate composition of gasses. Even with this method, there is still uncertainty in the RGA pressure estimates of the gasses. In addition, the RGA signal is based on the fraction of gases that are ionized and then make it through the quadrupole mass filter [9] and is not a true measure of partial pressure. It must be properly calibrated to the ionization efficiencies of the different gasses being analyzed which is influenced by the molecules' cross-sections. A similar complication arises

with the SRG as it is calibrated to nitrogen gas and the experiment is producing a gas mixture where the relative mass is not similar to that of nitrogen.

Chapter 3

Results

The results of this experiment will provide insight and guidance towards future experiments. The major results, thus far, are the production of H_3^+, data about the composition of the gasses outgassing from the AISI-1020 pipe, and how rate of rise changes with temperature. First off, through analyzing the standard RGA scans, there was a significant AMU 3 signal peak off of the AMU 2 peak. The two pressures were subsequently graphed over time and found a quadratic relationship between the two variables suggesting that as hydrogen gas increased so did H_3^+. This is shown in Fig. 3.1. This is believed to be H_3^+ because AMU 3 increases while AMU 2 decreases suggesting a chemical reaction converting two H_2 molecules into a H_3^+ molecule. Thus, as the H_2 pressure increased the H_3^+ pressure increased quadratically. Also, the AMU 3 is a much larger percentage of H_2 than if it contained a heavy isotope of hydrogen as H^2 makes up only 0.0115% of all hydrogen atoms and there is a quadratic relationship instead of linear [11].

Secondly, through analyzing the RGA plots like Fig. 2.4, the relative composition of the gasses in the pipe determined. Figure 3.2 displays that same plot as Fig. 2.4 but with a isotope and electron ionization simulation fit to the data as well. The fit was created using the relative abundance of carbon, hydrogen, and oxygen isotopes combined with the relative intensity of the various atomic masses for each gas

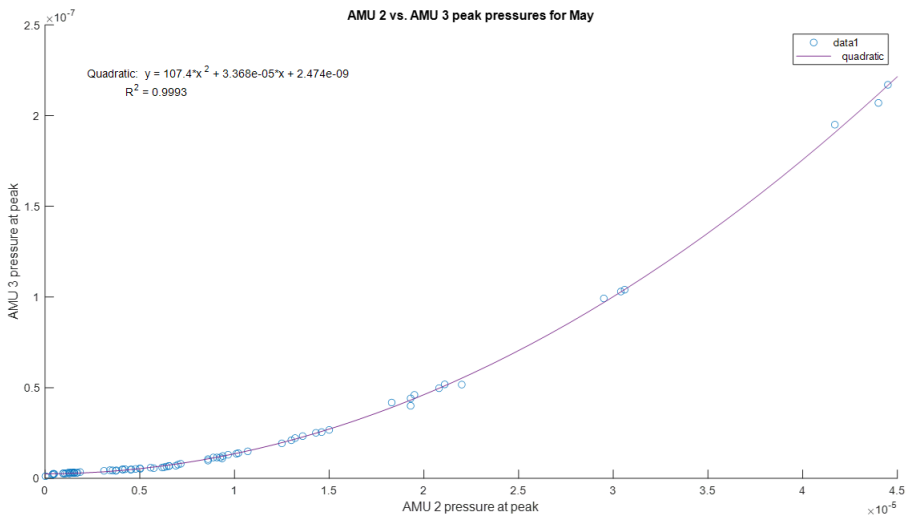

Figure 3.1: This figure displays the relationship between hydrogen gas (AMU 2) and H_3^+ (AMU 3) for data collected through the standard RGA scans in May. There appears to be a positive quadratic relationship between the two gases. This is believed to be caused by the collision between two H_2 molecules creating one H_3^+ molecule resulting in a positive quadratic relationship.

parameter used [7][10][11][12]. For Fig. 3.2 the gas parameters used are : H_2, CH_4, H_2O, CO, C_2H_6, and CO_2. The fitted curve closed matches the measured spectra indicating that the gas parameters make up most of the outgas and that the peaks are in fact the simulated gasses. The biggest discrepancy occurs at AMU 14 indicating that AMU 28 which is assumed to be CO, might be partially N_2 molecules as well that are unaccounted for in this fit. This is further suggested by peak 12 being lower than predicted suggesting less carbon due to the smaller CO peak.

After determining the major contributors to the mass spectra, the relative composition of the outgas at 21°C was determined. This was done by collecting RGA P vs. T data such as Fig. 2.5. Figure 3.3 displays the two pulses from Fig. 2.5 with a linear fit. This was used to estimate the initial pressure of each molecule by extrapolating back to time 0. The system changes rapidly and it is impossible to measure initial pressure due to the outgassing of molecules from the AISI-1020 pipe precisely, thus

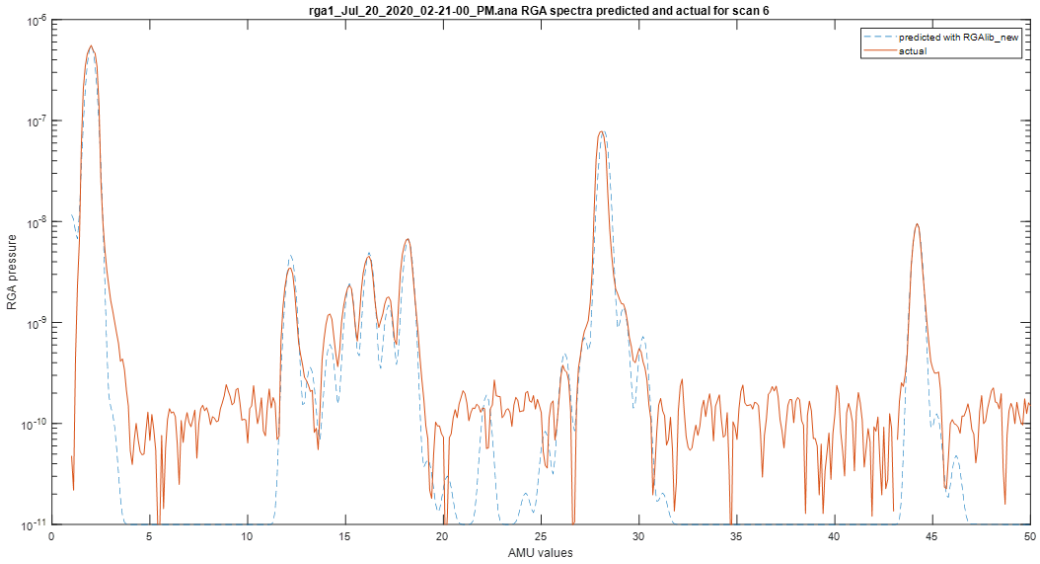

Figure 3.2: This is a sample plot displaying the RGA standard scan data and the corresponding isotope and electron ionization fit. The red solid line is the data collected by the RGA and the blue dotted line is the corresponding fit. This data is from July 20^{th} 2020 and is without correction for the cross-section of the molecules.

there is some uncertainty in these estimates. This process was repeated for AMU 15, 18, 28, and 44 through several pulses over several days one of which is shown in Fig. 3.4. Figure 3.4 also highlights how the system changes non-linearly for some AMU values as well. The initial pressures estimates were then calibrated using the cross-section ratios from Table 2.1 and averaged. This data spans from September 2020 to February 2021. The gas composition on average is shown in Table 3.1 and only displaying the portions of AMU 2, 28, and 44 as the other values were sufficiently small and insignificant.

Lastly, the SRG pressure data was also collected in the AISI-1020 pipe and measured each time the pipe gas was pulsed in. In terms of measuring the outgassing, the SRG rate of rise over time helps explain how quickly the products are outgassing and what affect temperature has on it. This is especially important because the SRG pressure has a nonlinear rate of rise initially after the valve pipe valve is closed, an

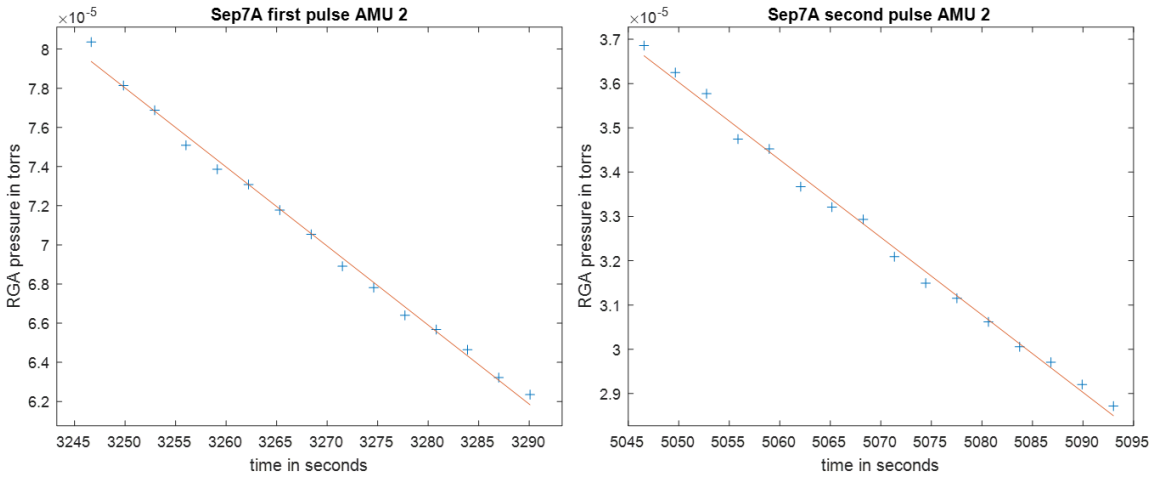

Figure 3.3: These graphs displays the two pulses from 2.5 with linear fit. The left is the first pulse and the right is the second pulse. These display that H_2 decreases approximately linearly with respect to time after the AISI-1020 gas is pulsed into the main chamber.

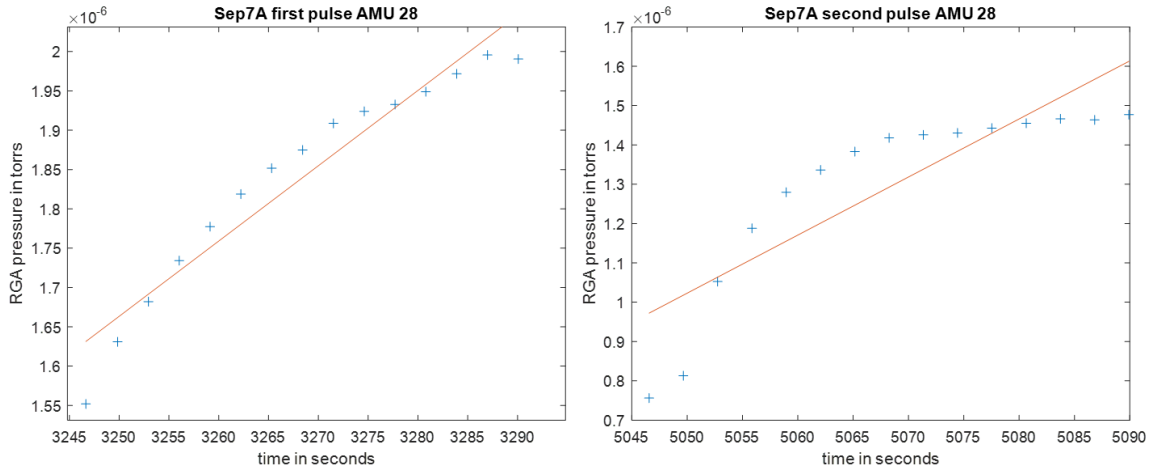

Figure 3.4: These graphs displays the two pulses for carbon monoxide with a linear fit. The left is the first pulse and the right is the second pulse. These display that CO increases non-linearly after the pipe gas is pulsed in. Estimating time 0 initial estimate required backwards extrapolating by following the data backwards.

AMU	Intensity (%)
2	99.22
28	0.65
44	0.13

Table 3.1: Estimate of Outgassing Composition at 21°C
This table displays the best estimate of the gas composition for the AISI-1020 pipe at 21°C. These values are based on the average ratios of the estimation of the initial gas pressure as determined from P vs. T RGA scans in September 7^{th}, 16^{th}, and 23^{rd}, December 21^{st}, January 11^{th}, and February 22^{nd}. The composition intensities are calculated after correcting the RGA initial pressure estimate for each molecule cross-section from Table 2.1.

example of which is shown in Figure 3.5. Once collected, the SRG rate of rise was calibrated to the relative mass of the system using the relative mass equation in Fig. 2.1. Table 3.2 displays an example of the raw SRG rate of rise collected for January 22^{nd}, the relative mass, and the corrected SRG rate of rise for various temperatures.

Once the overall SRG rate of rise is corrected, it can be separated out into the rate of rise of specific outgassing products using the proportion each gas makes up for the total gas. This is done by multiplying the corrected SRG ROR by the proportion of each gas to find the ROR of each individual gas. These calculations are assuming that hydrogen gas, carbon monoxide, and carbon dioxide make up the total outgassing because all of the other components are small and insignificant for our purposes. One of this data tables displaying this process is shown in Table 3.3. The corrected rate of rise for this example is 1.58E-07 Torr/hr. This analysis was than repeated for each pulse 1 and 2 at 21, 40, 50, 60, 70, and 80°C. The data is summarized in Table 3.4. Figure 3.6 displays the individual rate of rise on a semilog plot vs. the Inverse Temperature of each experiment as well as the model that represents the data. This model is: $ROR = Ce^{E/kT}$ where E is the binding energy, k is Boltzmann's constant (8.617E-05 eV/K), T is Temperature in Kelvin, and C is based on 40°C to scale the values appropriately. The equations for these calculations are in Figure 3.7.

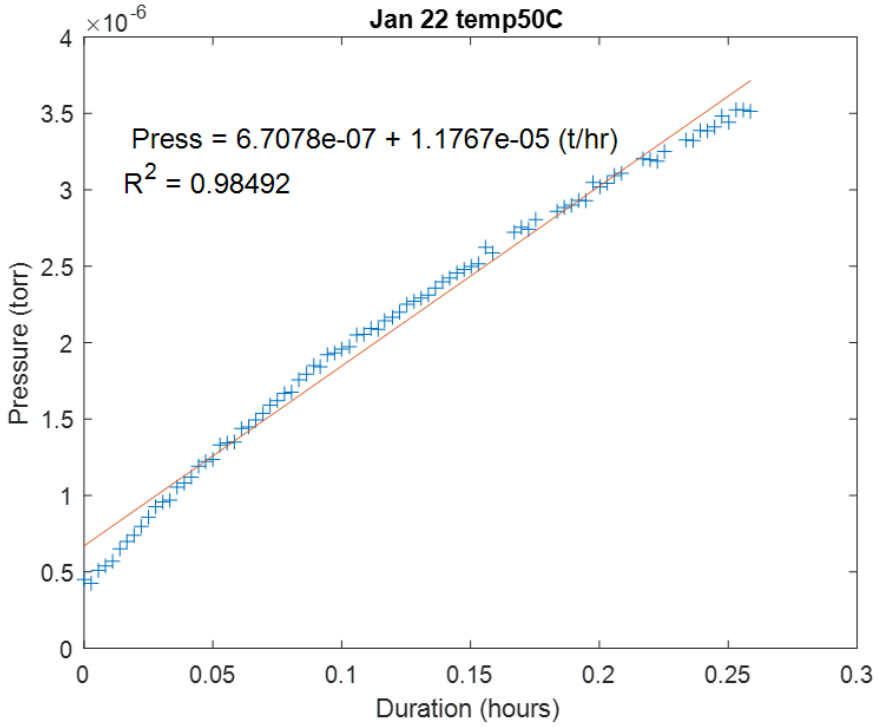

Figure 3.5: This plot displays an example of the nonlinear behavior of the SRG pressure after the pipe valve was closed. This particular run occurred on January 22^{nd} with the pipe at 50° Celsius.

	Temperature	Raw SRG ROR (Torr/hr)	relative mass (AMU)	corrected SRG ROR (Torr/hr)
Jan. 22 1st	21° C	4.37E-08	2.14	1.58E-07
Jan. 22 2nd	21° C	4.37E-08	2.15	1.58E-07
Jan. 22 1st	40° C	7.26E-07	3.72	1.99E-06
Jan. 22 2nd	40° C	7.26E-07	3.88	1.95E-06
Jan. 22 1st	50° C	9.39E-06	14.68	1.30E-05
Jan. 22 2nd	50° C	9.39E-06	15.07	1.28E-05
Jan. 22 1st	60° C	5.99E-05	31.68	5.64E-05
Jan. 22 2nd	60° C	6.42E-05	26.81	6.56E-05
Jan. 22 1st	70° C	2.45E-04	29.40	2.39E-04
Jan. 22 2nd	70° C	2.68E-04	27.27	2.72E-04
Jan. 22 1st	80° C	9.68E-04	33.34	8.87E-04
Jan. 22 2nd	80° C	1.08E-03	30.67	1.03E-03

Table 3.2: SRG Rate of Rise for January 2021

This table displays the SRG Rate of rise at various temperatures on January 22^{nd}, 2021. The first column represents the day and pulse number with "1st" indicating the first pulse and "2nd" indicating the second pulse. The SRG rate of rise is determined by the slope of the SRG pressure vs. time graphs like Fig. 2.3 and 3.5. For SRG that rose non-linearly, the long-term linear behavior was used. The relative mass was calculated using the equation in Fig. 2.1. This was used to calculated the corrected SRG ROR by multiplying the raw SRG ROR by the squareroot(28/relative mass) because the SRG is calibrated to N_2 with AMU of 28.

AMU	Raw RGA (Torr)	Calibrated RGA (Torr)	Proportion	Rate of Rise (Torr/hr)
2	4.92E-06	1.21E-05	98.82%	1.56E-07
28	1.24E-07	1.23E-07	1.01%	1.60E-09
44	2.96E-08	2.11E-08	0.17%	2.73E-10

Table 3.3: Example Rate of Rise for Individual Gasses

This table displays an example of the individual ROR for each outgassing component. The second column is the pressure in Torr as measured by the RGA right after the first pulse. The third column is the calibrated pressure using the cross-section ratios in Table 2.1. The last column is the rate of rise of each component based on the proportion of each gas to the total. This is using the corrected SRG for this pulse which is 1.58E-07 Torr/hr based on the calculated relative mass of 2.14 AMU using the equation in Fig. 2.1.

January 22nd, Pulse 1			
Temperature in Kelvin	AMU 2 ROR (Torr/hour)	AMU 28 ROR (Torr/hour)	AMU 44 ROR (Torr/hour)
21	1.56E-07	1.60E-09	2.73E-10
40	1.77E-06	9.42E-08	1.26E-07
50	6.54E-06	1.62E-06	4.80E-06
60	8.57E-06	8.87E-06	3.89E-05
70	4.36E-05	4.63E-05	1.49E-04
80	1.10E-04	1.42E-04	6.36E-04
January 22nd, Pulse 2			
Temperature in Kelvin	AMU 2 ROR (Torr/hour)	AMU 28 ROR (Torr/hour)	AMU 44 ROR (Torr/hour)
21	1.56E-07	1.66E-09	3.11E-10
40	1.72E-06	8.94E-08	1.41E-07
50	6.38E-06	1.44E-06	4.98E-06
60	1.54E-05	1.12E-05	3.89E-05
70	6.24E-05	4.33E-05	1.66E-04
80	1.70E-04	1.79E-04	6.79E-04
February 11th, Pulse 1			
Temperature in Kelvin	AMU 2 ROR (Torr/hour)	AMU 28 ROR (Torr/hour)	AMU 44 ROR (Torr/hour)
21	2.17E-07	4.36E-10	7.04E-11
40	1.76E-06	2.04E-08	1.37E-08
50	1.06E-05	6.03E-07	1.22E-06
60	2.58E-05	5.12E-06	1.35E-05
70	3.22E-06	3.58E-05	9.35E-05
80	2.51E-05	1.38E-04	4.07E-04
February 11th, Pulse 2			
Temperature in Kelvin	AMU 2 ROR (Torr/hour)	AMU 28 ROR (Torr/hour)	AMU 44 ROR (Torr/hour)
21	2.16E-07	5.00E-10	1.15E-10
40	1.74E-06	2.23E-08	1.67E-08
50	9.63E-06	7.11E-07	1.33E-06
60	2.07E-05	3.70E-06	1.60E-05
70	1.56E-05	3.15E-05	8.14E-05
80	1.89E-05	1.27E-04	3.34E-04

Table 3.4: Individual Gas Rate of Rise For January 22^{nd} and February 11^{th} at Various Temperatures
This table displays the calculated ROR for each of the significant outgasses using the relative mass, raw SRG data, and proportions of the gasses. This data is plotted in Fig. 3.6

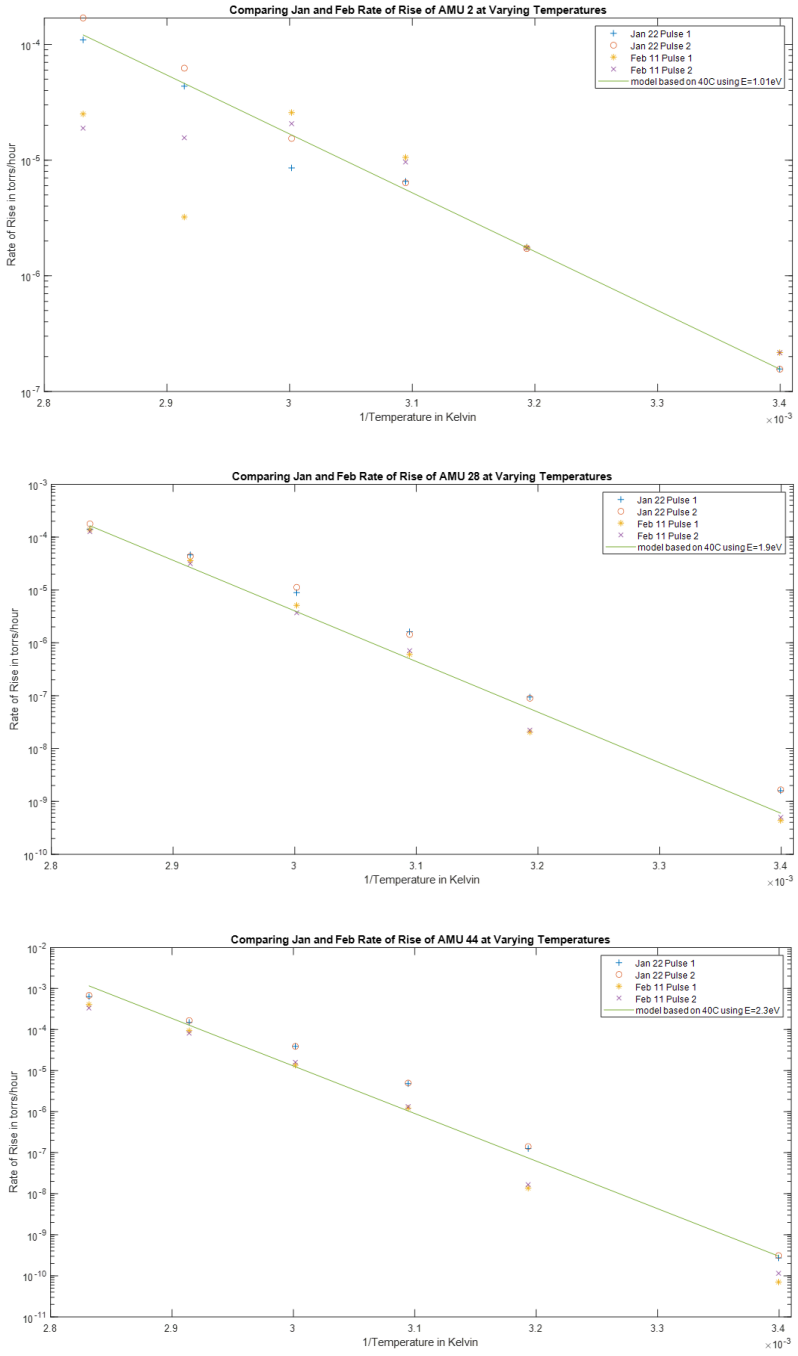

Figure 3.6: This figure displays the ROR for each individual gas as a function of Inverse Temperature in 1/Kelvin. Each plot also has an overlay of a model of $ROR = Ce^{E/kT}$ where C is the scale factor determined by 40°C and E is the calculated binding energy. Both calculations are shown in shown in Fig. 3.7.

$$\mathrm{ROR} = e^{-\frac{E}{kT}}, \qquad k = 8.617E-05 \ eV/K$$

$$\log_{10}(ROR) = \log_{10}\left(e^{-\frac{E}{kT}}\right)$$

$$\log_{10}(ROR) = \log_{10}(e)\frac{-E}{kT}$$

$$\log_{10}(ROR) = \left(\frac{-E}{kT}\right)\frac{1}{2.302}$$

$$E = (-\log_{10}(ROR)) * 2.302 * kT$$

$$E = -m * 2.302 * k$$

$$m = slope = \left(\log_{10}(ROR)\right)/(1/T)$$

$$C = ROR_{313.15K}\left[e^{E\left(\frac{1}{k(313.15K)}-\frac{1}{kT}\right)}\right]$$

Figure 3.7: These equations explain how the Binding energy for each AMU value is calculated from the graphs in Fig. 3.6. The binding energy was calculated by multiplying the slope produced when plotting the log10(ROR) over 1/T. To further confirm this calculation, the binding energy was modeled using 40°C by functionally calculating the y-offset for the data as represented by C. In the C equation, $\mathrm{ROR}_{313.15K}$ is the average ROR value at °C based on the data from Table 3.4

Chapter 4

Conclusion and Outlook

Based on the results there are four major conclusions of the experiment so far: H_2 produces H_3^+ in the presence of the RGA filament, the AISI-1020 pipe is outgassing mostly hydrogen, carbon monoxide, and carbon dioxide gasses, as temperature increased the outgassing increased and carbon dioxide became the dominant gas, and the binding energy for each of the three gasses was determined based on the ROR of individual gasses. First, based on the strong quadratic relationship between AMU 2 and AMU 3 as seen in Fig. 3.1, the system is likely undergoing a chemical reaction where H_2 is converted into H_3^+ due to the heated filament used in the RGA. This is one of many chemical reactions and is the best understood so far. These chemical reactions modify the relative intensities of the various gasses thus extrapolating to time 0 provides a better estimate of the initial pressure and thus the relative intensities. Secondly, the gasses contributing the most to the outgassing are hydrogen, carbon monoxide, and carbon dioxide with hydrogen making up the vast majority at low temperatures. However, hydrogen is a small molecule and of minimal concern to LIGO therefore, CO_2 and CO are the major concerns moving forward. This result is also interesting as there is a low water vapor (AMU 18) outgassing rate which is inconsistent with the data from Fred Dylla (private communication). The experiment data presented here also reports much smaller relative intensities compared to

hydrogen overall compared to the data from Fred Dylla (private communication).

Thirdly, when studying the system at different temperatures the total outgassing rate of rise increased as shown in Table 3.2 and carbon dioxide became the most prominent gas suggesting that at higher temperatures more carbon dioxide was being released possibly due to the binding energies of each gas. The exact reasons why this is occurring still needs to be further studied. Lastly, the binding energy of each gas to be calculated using the equations in Fig. 3.7 and the slope from each graph in Fig. 3.6. The calculated binding energy of each gas is shown in Table 4.1 suggesting that heavier molecules are more tightly bond to the metal.

	Binding Energy
Hydrogen Gas	1.0eV
Carbon Monoxide	1.9eV
Carbon Dioxide	2.3eV

Table 4.1: Binding Energy for the Major Outgassing Components
This table displays calculated binding energy for each of the major outgassing components based on the slopes from Fig. 3.6 based on data from January and February of 2021 as calculated using the equation in Fig. 3.7. The binding energy of AMU 2 is calculated only using the data from January 22 because AMU 2 for February had high uncertainty in determining initial pressure in the AISI-1020 pipe.

Moving forward, this experiment will focus on temperature studies on the AISI-1020 pipe and further understanding the system. The temperature studies will consist of baking the pipe at incrementally increasing temperatures to determine how temperature affects outgassing both during the bake and afterwards. Figure 4.1 shows the long term outgassing rates as measured by the SRG over several months. When the SS316 was baked the outgassing rate dropped significantly afterwards, therefore there is reason to believe the same will occur with the AISI-1020 pipe. This is still multiple components of this system that we do not understand fully such as the chemistry going on in the presence of filaments, the presence of a black coating that may be

altering the outgassing rates of different gasses, the short-term nonlinear SRG rate of rise that occurs, or why carbon dioxide becomes the most prominent outgas at higher temperatures. These are all aspects that can be further explored in future research.

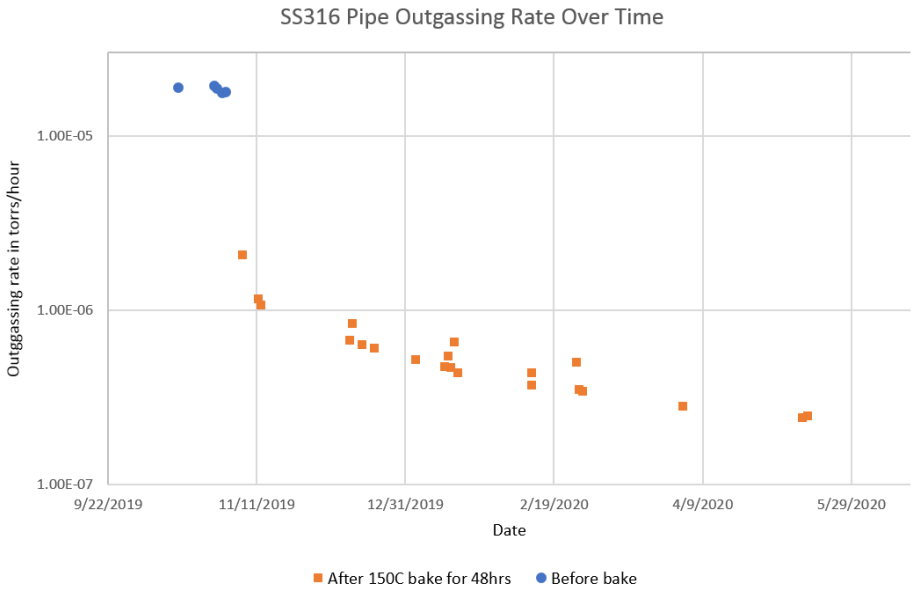

Figure 4.1: This figure displays the outgassing rates over time for the SS316 pipe as measured by the SRG. There is a significant decrease in the outgassing rate after baking the pipe at 150°C for 2 days. This plot was created by Dr. William Cooke.

Bibliography

[1] Cosmic Explorer. (n.d.). Retrieved April 30, 2021, from https://cosmicexplorer.org/

[2] Factory Directly 2 Meter Large Diameter SSAW Steel Pipe Tube ASTM A53 With Epoxy Paint Coating. (n.d.). Retrieved April 30, 2021, from https://www.alibaba.com/product-detail/Factory-Directly-2-Meter-Large-Diameter_1600158665291.html?spm=a2700.7724857.normal_offer.d_title.c82f3731YXCJbn

[3] Kim, Y.-K., Irikura, K.K., Rudd, M.E., Ali, M.A., Stone, P.M., Chang, J., Coursey, J.S., Dragoset, R.A., Kishore, A.R., Olsen, K.J., Sansonetti, A.M., Wiersma, G.G., Zucker, D.S., and Zucker, M.A. (2004), Electron-Impact Ionization Cross Section for Ionization and Excitation Database (version 3.0). [Online] Available: http://physics.nist.gov/ionxsec [2021, April 7]. National Institute of Standards and Technology, Gaithersburg, MD.

[4] LIGO Scientific Collaboration. (n.d.). LIGO - A Gravitational-Wave Interferometer. Retrieved April 30, 2021, from https://www.ligo.caltech.edu/page/ligo-gw-interferometer

[5] MKS Instruments Deutschland GmbH. (2004). SRG - 2 CE/O Spinning Rotor Vacuum Gauge Instruction Manual (03/2004).

[6] MKS: SRG -3 Spinning Rotor Vacuum Gauge Instruction Manual. 2012-08 ed. MKS Instruments Deutschland GmbH, 2009. Print.

[7] NIST Mass Spectrometry Data Center, William E. Wallace, director, "Mass Spectra" in NIST Chemistry WebBook, **NIST Standard Reference Database Number 69**, Eds. P.J. Linstrom and W.G. Mallard, National Institute of Standards and Technology, Gaithersburg MD, 20899, https://doi.org/10.18434/T4D303, (retrieved November 16, 2020).

[8] Stainless 316L 304 1200mm diameter steel pipe. (n.d.). Retrieved April 30, 2021, from https://www.alibaba.com/product-detail/Stainless-316L-304-1200mm-diameter-steel_62318078474.html?spm=a2700.7724857.normal_offer.d_title.76214d3ct2PXlD

[9] Stanford Research Systems, Inc. (2009). Chapter 2: RGA General Operation. In Models RGA100, RGA200, and RGA300 Residual Gas Analyzer: Operating Manual and Programming Reference (pp. 34–45).

[10] Thomas Jefferson National Accelerator Facility - Office of Science Education. (n.d.). Isotopes of the Element Carbon. Retrieved November 20, 2020, from https://education.jlab.org/itselemental/iso006.html

[11] Thomas Jefferson National Accelerator Facility - Office of Science Education. (n.d.). Isotopes of the Element Hydrogen. Retrieved November 16, 2020, from https://education.jlab.org/itselemental/iso001.html

[12] Thomas Jefferson National Accelerator Facility - Office of Science Education. (n.d.). Isotopes of the Element Oxygen. Retrieved November 16, 2020, from https://education.jlab.org/itselemental/iso008.html